Chapter 4

Photometric Characterization and Spectral Validation of *SUIT*

'...nobody in their right mind would let an astronomer touch the controls of one of the most powerful telescopes on earth.'

— Richard Preston, *First Light.*

SUIT is designed to deliver relative photometric measurements within 1% accuracy from one spatial location to another in an image. To achieve the scientific goals, photometric and spectral calibration of the payload is of utmost importance. This chapter provides a complete account of the calibration procedure while discussing the experimental setup and contamination control in detail for *SUIT*.

The model details and derived design values are discussed in §4.1. The telescope is calibrated for throughput accuracy during the final test before integration on the satellite. Details of the calibration setup are explained in §4.2. The results from in-lab calibration and its comparison with the design values are shown in §4.3 and §4.4.

This thesis chapter originally appeared in the literature as– **Sarkar, J.**, Roy, S., Ramaprakash, A. N. et al. *Photometric calibration and spectral validation of the Solar Ultraviolet Imaging Telescope onboard Aditya-L1*, Journal of Astronomical Telescopes, Instruments, and Systems 11(1), 014005 (2025). https://doi.org/10.1117/1.JATIS.11.1.014005

4.1 Telescope Throughput Model

SUIT telescope design is performed considering the requirement of throughput and photometric accuracy. Optical parameters of different optical components, like reflectivity of the primary and secondary mirrors, thermal filter transmission, field corrector lens transmission, spectral transmission of the science filter, and the combination filter, are tuned to deliver the best possible throughput at corresponding wavelength ranges.

The end-to-end optical response of the instrument is modeled from the lab-measured parameters (transmission, reflectivity, quantum efficiency) of each component using Equation 4.1. We use the concatenated solar spectral irradiance from SOLar STellar Irradiance Comparison Experiment (SOLSTICE; 115–320 nm) onboard the SOlar Radiation and Climate Experiment (SORCE) [20–22] satellite and SOLar SPECtrometer (SOLSPEC; $>$ 320 nm) [23], along with the optical response, to predict the expected signal. Note that in this wavelength range ($>$ 320 nm), SOLSPEC offers the best available wavelength resolution measurements, and is therefore used for our work. The concatenated spectrum is interpolated to the same spectral resolution as that of the corresponding science filter spectral measurements. This is necessary to decide the exposure times of the payload in the eleven science bandpasses for various modes of operation.

$$\mathrm{DN} \;=\; \int_{\lambda_1}^{\lambda_2} \mathrm{P}(\lambda)\ \mathrm{R}(\lambda)\ \mathrm{t}\ \mathrm{d}\lambda \tag{4.1}$$

Here,

- P(λ)= Incoming photon flux (Photons $\mathrm{m}^{-2}\mathrm{s}^{-1}$) from the Sun falling on the entrance aperture of *SUIT*. The total number of photons is integrated over a wavelength range of 200 nm to 1000 nm. This is derived from the solar spectral irradiance (SSI) from the concatenated SORCE-SOLSTICE and SOLSPEC spectra in units of $Wm^{-2}nm^{-1}$. The SSI is divided by photon energy (hc/λ) of the corresponding wavelength to derive the number of incident photons for that particular wavelength bin. This is in units of the number of photons.

- t= Exposure Time in seconds.
- R(λ)= Effective Area of the end-to-end configuration of *SUIT* for a particular science filter combination. This is derived by multiplying the measured transmittance/reflectance of all the optical sub-assemblies in the beam path, along with the sensitivity and analog to digital conversion of the CCD and its electronics. This can be expressed as-

$$\mathrm{R}(\lambda) = \mathrm{TF}(\lambda) \times \mathrm{PM}(\lambda) \times \mathrm{SM}(\lambda) \times \mathrm{SF_i}(\lambda) \times \mathrm{SF_j}(\lambda) \times \mathrm{L}(\lambda) \times \mathrm{QE}(\lambda) \times \mathrm{G} \times \mathrm{A} \tag{4.2}$$

  where the measured dimensionless spectral profiles, and the corresponding spectral step size (in parentheses) are given as,

  - TF(λ)= Thermal filter at entrance aperture (5 nm).
  - $\mathrm{SF_i}(\lambda)$ and $\mathrm{SF_j}(\lambda)$= Science filters (0.01– 0.02 nm for various filters).
  - L(λ) = Field correction lens (5 nm).
  - PM(λ) and SM(λ)= Primary and Secondary mirrors (1 nm).
  - QE(λ) : CCD quantum efficiency (Photoelectrons: pe^-).
  - G= CCD electronics gain ($^{DN}/_{pe^-}$)
  - A= Area of the telescope aperture in m^2.

  For further operations, the quantities are interpolated to the smallest spectral sampling rate of all measurements so as to resolve various spectral features observed to be observed by *SUIT*.

The incoming rate of photon flux (P(λ)) is multiplied by the telescope response function (R(λ)) and exposure time. This is integrated over the wavelength band of interest (between λ_1 and λ_2) to simulate the data numbers detected by *SUIT* in a particular filter combination. The effective area curves for each filter are shown in Fig. 4.1.

4.2 Experimental Setup

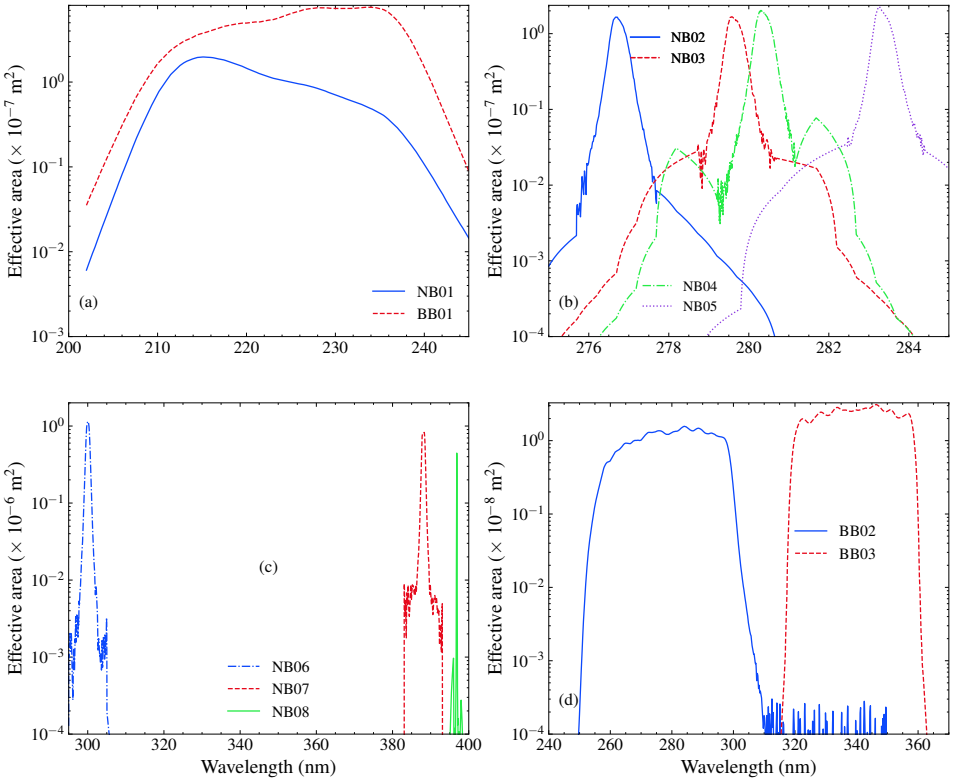

Figure 4.1: The effective area curves for *SUIT* science filters. The central wavelengths and the observation interest for each bandpass are tabulated in Table 1.2.

An experimental setup is developed, as illustrated in Figure 4.2, to measure the end-to-end throughput of the instrument and compare the measured results with the throughput model described in §4.1. Light of known spectral irradiance is fed into the payload from a monochromator after collimation. The payload is operated in a vacuum chamber to simulate space-like conditions in this setup.

4.2.1 Contamination control and payload preparation

Given the operational wavelength range, the throughput of *SUIT* is highly susceptible to particulate and molecular contamination. Therefore, it is assembled and stored in a Class 100 clean room with constant purging of 5.0 purity gaseous nitrogen. In space, the *SUIT* CCD is passively cooled to – 55° C with a radiator plate and a cold finger. To attain the same level of cooling in lab, the payload is operated in a contamination-controlled 0.7 m custom-made vacuum chamber at a pressure of $< 10^{-6}$ mbar. Liquid nitrogen is fed by closed-loop micro-dosing through a cooling jacket mounted over the CCD heat pipe, instead of using the radiator plate.

Before loading the payload, the vacuum chamber is cleaned with isopropyl alcohol and baked at 70°C for 24 hours. Temperature Controlled Quartz Crystal Microbalance (TQCM) verification is performed with the crystal at -10° C in high vacuum. Frequency change of ≤ 3 Hz/hr over 24 hours was considered satisfactory for operating *SUIT* in the chamber. However, in practice < 2 Hz/hr was achieved over 36 hours. This corresponds to a contaminant deposition rate of 3.92×10^{-9} g/cm^2/Hr on the TQCM crystal ($1Hz/hr \equiv 1.96 \times 10^{-9}$g/cm^2/hr).

The photometric and spectral calibration of *SUIT* is performed after payload vibration, acoustic, and thermovacuum qualification tests. This required transportation of the payload to various clean rooms and labs. To avert any risk of contaminating the CCD upon cooling, the payload is subjected to a bake-out at 40° C for 36 hours after loading in the chamber. TQCM verification is ensured to be $<$ 3 Hz/hr over 24 hours after payload baking.

4.2.2 *SUIT* Collimator

The *SUIT* flight spare is used as a collimator because of comparable optical performance as the payload in NUV. An illuminated target is kept at the focal plane, light from which emerges collimated from the front aperture. The *SUIT* collimator exhibits an RMS wavefront error of 41.4 nm ($\approx \lambda/7\ for\ 300\ nm$) as compared to the *SUIT* payload's 34 nm ($\approx \lambda/9\ for\ 300\ nm$). The Zernike coefficients of the collimator and the payload are tabulated in Table 3.1. The collimator is mounted on an optical table so that the front aperture is aligned with the viewport of the vacuum chamber housing the *SUIT* payload as in Fig 4.2. The optical bench is designed to rest on six pods bolted to the optical table. The telescope and collimator are of RC design, causing the wavefront error to change grossly in case of stress-induced misalignment. Therefore, all bolts are uniformly and gradually torqued to 400 N-cm to avoid mechanical distortion of the optical bench while ensuring planarity with a feeler gauge and filling any gaps between the pods and the bench with appropriate shims.

A big flat mirror (dia: 150 mm) is placed at the front aperture of the collimator along the payload optical axis. The collimator's wavefront error is verified with a Fizeau Interferometer by focusing an f/25 beam at the focal plane and retro-reflecting it from the reference mirror at the front aperture, to ensure proper mounting. Following this, an f/3.5 transmission sphere is used with the interferometer to overfill the mirrors of *SUIT* collimator. Repeated interferograms are taken, and the fringes are constantly monitored while the interferometer is moved along the optic axis. This is done till the fringes appear straight instead of circular, indicating nullification of power. The point of convergence of the beam from the interferometer is the focal point of the collimator, indicating the location for a target.

Light from the collimator is fed into the vacuum chamber through an Allectra Deep UV Viewport (110-VPQZ-C200-DUV) which provides $> 99.8\%$ internal transmission at 248 nm, ensuring nearly complete transmission inside the glass. However, $\approx 4\%$ of the light reaching each surface is lost due to reflection. The light entering the chamber is focussed and imaged by *SUIT*. To avoid any light loss, aligning the lateral position and tilt of the payload with the collimator is necessary. This alignment of the collimator and the payload is achieved with a theodolite, which also functions as an autocollimator.

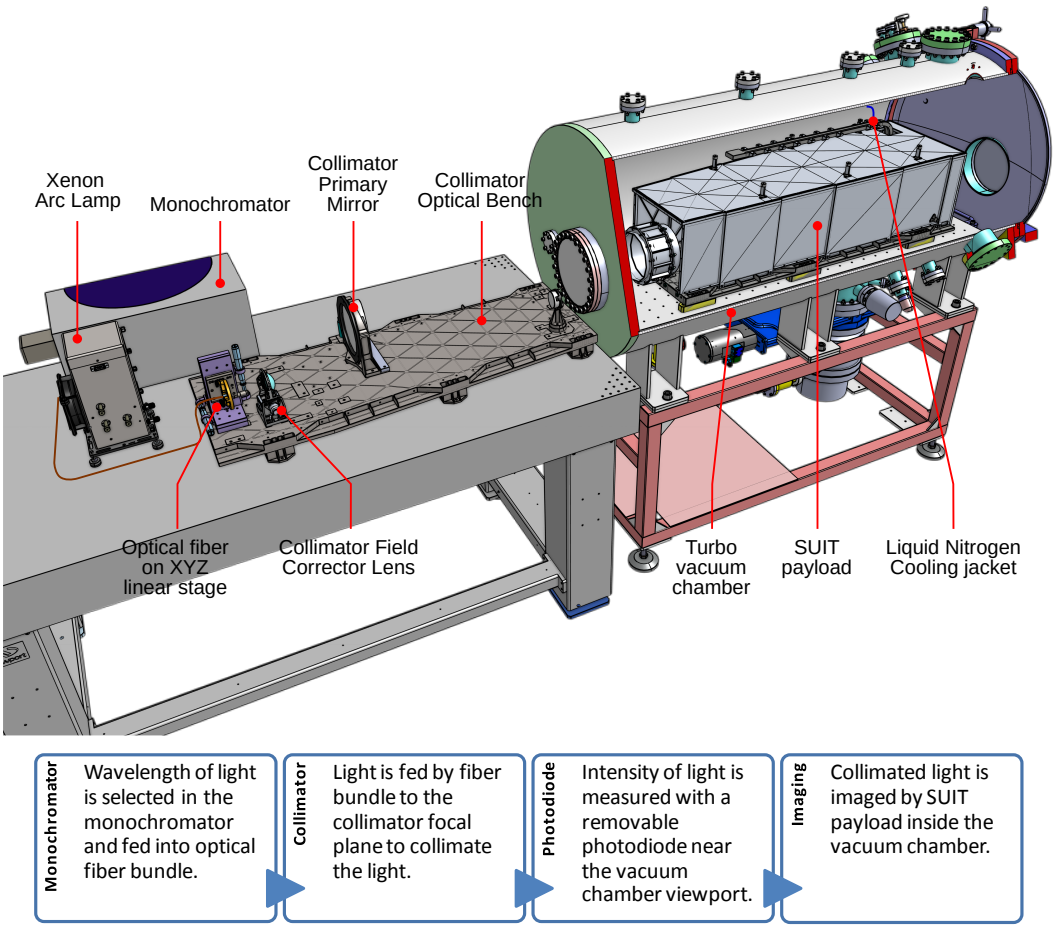

Figure 4.2: Diagram [top] and schematic flowchart [bottom] for photometric calibration and spectral validation of *SUIT* showing the section view of the turbo vacuum chamber.

The theodolite is autocollimated with the Collimator axis using the reference mirror. With assistance from repeater mirrors and theodolite, the axes of the collimator are matched with that of the payload. The optical axis of *SUIT* is given by a reference cube placed on the optical bench, outside the cover panel. The payload is finely shifted within the vacuum chamber to achieve autocollimation with the alignment cube. This aligns the payload in the vacuum chamber with the collimator facing it outside the vacuum chamber.

4.2.3 Monochromator configuration and calibration

For photometric and spectral calibration, collimated light from a known wavelength band and intensity is fed into the payload. For this purpose, we use Andor Shamrock 500i spectroscope/ monochromator with an optical fibre (Andor SR-OPT-8024). One end of the optical fiber bundle forms a linear array with 19 fibers of 0.2 mm thickness. This end is attached to the monochromator and behaves like an exit slit with a thickness of 0.2 mm and height 4.655 mm. The other end of the fibre forms a circular bundle and is placed at the focal plane of the collimator.

A Mercury light source (Ocean Optics HG2 Wavelength Calibration Source) is used for wavelength calibration of the monochromator. The Mercury lamp is kept at the entrance aperture, and the monochromator is set to observe a relatively isolated spectral line at 253.65 nm. Using a micrometer actuator, the position of the fiber slit is adjusted to get maximum intensity at the fiber face. This is validated with another relatively isolated line (365 nm) within the 200–400 nm band. The mercury lamp is then replaced with a Xenon Arc Lamp (75W Newport 60000 Q Series Lamp with stabilized power supply), which is focused at the input slit of the monochromator.

4.3 Photometric Calibration

In this test, an optical fiber is used to feed light from the monochromator at the focal plane of the *SUIT* collimator, as shown in Fig 4.2. The monochromator uses 1200 lines per mm (lpmm) grating with a nominal dispersion of 1.44 nm/mm, blazed at 500 nm. The spectral resolution of the monochromator depends on the entrance slit or the exit slit, whichever is geometrically wider. In our case, an entrance slit width of 3 mm is used to maximize the light output from the spectroscope, delivering wavelength band of 4.32 nm. This wavelength band accommodates the complete transmission spectrum of all the narrowband science filters (Table 1.2) being tested.

A UV-enhanced National Institute of Science and Technology (NIST) traceable photodiode (Newport 918D-UV-OD3R) is kept at the exit aperture of the collimator, which measures the net collimated output flux (in $nWcm^{-2}$)

Science filter	**Counts calculated from measurement** $DN_m = E_\odot \times F$ $(Data\ number\ s^{-1})$	**Counts calculated from throughput model** $DN_t = \int P(\lambda)\ R(\lambda)\ t\ d\lambda$ $(Data\ number\ s^{-1})$	**Ratio** $\frac{DN_m}{DN_t}$
NB02	57763	49099	1.18
NB03	20142	15520	1.3
NB04	38087	36717	1.04
NB05	134909	131625	1.02
NB06	114280	107064	1.07
NB07	816026	391364	2.09
NB08	28829	24096	1.2
BB03	556220	434532	1.28

Table 4.1:: Comparison of the data numbers derived from throughput model (using SOLSTICE and SOLSPEC data) with the data numbers inferred from the measurements. DN_m: Measured Data Numbers. DN_t: Data Numbers derived from throughput model.

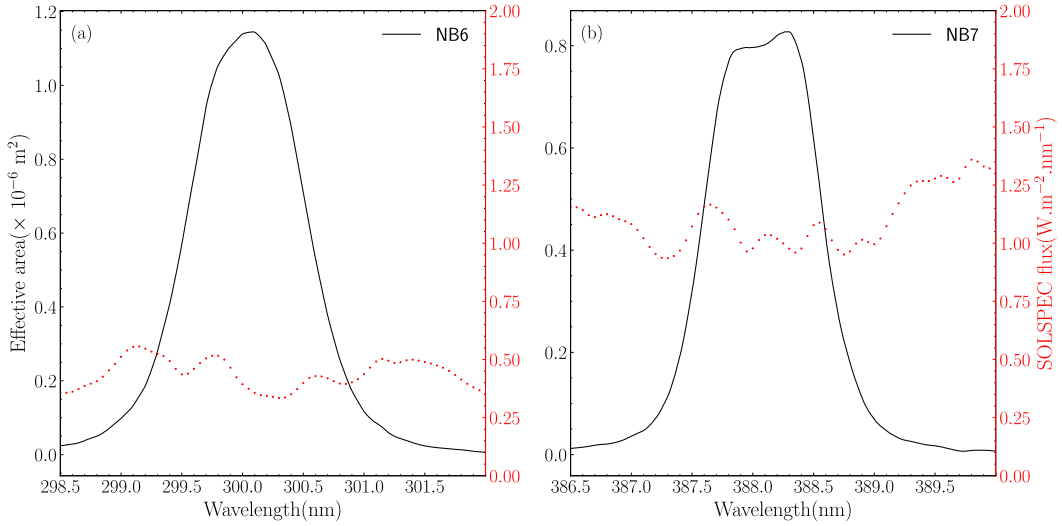

Figure 4.3: Spectral transmission profile of *SUIT* in (a) NB06 and (b) NB07 bands with solar spectrum from SOLSPEC data.

falling on the photodiode with area $1cm^2$. An average of 150 independent readings are taken in a time span of 10 seconds. The monochromator's and photodiode's wavelengths are set based on the science filter being tested.

The power measured with the photodiode (nW) is normalized by the collecting area (nWm^{-2}) and divided by the wavelength band of the spectrograph to get the spectral flux from the collimator (in $Wm^{-2}nm^{-1}$). The xenon light intensity changes linearly within this wavelength band, making it viable to divide the photodiode output by 4.32 nm to get the spectral flux. Also, the incoming wavelength band is wide enough to accommodate the entire transmission spectrum of the narrowband science filters (typically $< 1\ nm$ FWHM). Therefore, the wavelength band incident from the monochromator is sufficient to perform the photometric test with the *SUIT* payload. The photodiode reading is recorded. Following this, the fiber face at the collimator is covered, and the background value seen on the photodiode is recorded. Finally, the photodiode is removed from the beam path, and an image of the fiber bundle is taken with *SUIT*. The fiber face is covered to record the background value, and another exposure is taken. These results can be directly compared with the modeled throughput derived from the sun-as-a-star spectrum for various filter wavelength bands. The measurements are not affected by out-of-band transmissions, such as those arising from higher grating orders. The *SUIT* science filters transmit only 0.01% - 0.001% out-of-band radiation, significantly cutting out wavelengths beyond the desired bandpass (Table 1.2). In addition, our longest test wavelength is $\approx 396.9nm$. The second order contamination, if at all, would arise from $\approx 200nm$. Since we operate the collimator in air, these higher-order wavelengths are heavily attenuated. We were unable to detect emission below $\approx 250nm$, even in the first order.

The setup illustrated in Fig. 4.2 is employed for the test. We can predict the solar throughput in various passbands from the experiment results and compare them with the modeled throughput derived from the sun-as-a-star solar spectrum using,

$$\mathrm{R} = \frac{\frac{\mathrm{DN}_{0.99}}{\mathrm{E}_{0.99}} \times \mathrm{E}_{\odot}}{\mathrm{DN}_{\mathrm{simulated}}} \text{ where,} \tag{4.3}$$

$\mathrm{DN}_{0.99}$ = Data number per second within 99% enclosed counts raidus of the fiber image ($\mathrm{DN.s^{-1}}$)

$$\mathrm{E}_{0.99} = \frac{Photodiode\ Output\ [nWm^{-2}]*0.92*\Delta\lambda[nm]}{4.32\ nm}\ (\mathrm{nW.m^{-2}})$$

Measured input flux from the photodiode in the bandpass [$\Delta\lambda$] of the concerned filter.

Corrected for reflective losses at viewport surfaces.

$$\mathrm{E}_{\odot} = \int_{\lambda_1}^{\lambda_2} P(\lambda)\ d\lambda\ (nW.m^{-2})$$

Incident energy from a sun as a star spectrum in the concerned filter's passband.

$$\mathrm{DN}_{\mathrm{simulated}} = \int_{\lambda_1}^{\lambda_2} P(\lambda)\ R(\lambda)\ t\ d\lambda\ (In\ units\ of\ DN.s^{-1})$$

Predicted data number from a sun as a star spectrum using the throughput model

We calculated the quantities in Eqn. 4.3 using the following steps:

- The background count is estimated by taking the median of the fiber occulted image.
- From the background corrected optical fiber images, we calculate the total counts within 99% enclosed counts radius. We use 99% to ensure we collect most of the light from the fiber ($\mathrm{DN}_{0.99}$).
- We use the concatenated SOLar STellar Irradiance Comparison Experiment (SOLSTICE; 115–320 nm) onboard the SOlar Radiation and Climate Experiment (SORCE) [20–22] satellite and SOLar SPECtrometer (SOLSPEC; $>$ 320nm) [23] solar spectrum as our standard for solar radiation. Using the spectra, we calculate the total energy input from the Sun for the concerned filter within the wavelength extent, $\mathrm{E}_{\odot}$.
- The photodiode gives the measurement of the corresponding input flux

for an input spectral bin of 4.32 nm. This is used to calculate the input flux in the bandpass of the concerned filter,

$$\mathrm{E}_{0.99}(\text{in units of nW.m}^{-2}) = \frac{Photodiode\ Output\ [nWm^{-2}]*0.92*\Delta\lambda[nm]}{4.32\ nm}$$

$\approx 4\%$ of the flux reaching each viewport surface is lost to reflection. This is accounted for by the factor of ≈ 0.92.

- Using Eqn.4.1 along with the aforementioned spectrum, we can now calculate the expected counts observed (i.e., $\mathrm{DN}_{\mathrm{simulated}}$(in units of DN.s^{-1}) for a given filter combination.

In Table 4.1, we list the comparison between the solar counts inferred from our measurements and the counts calculated from the throughput model for some of the filter combinations. Note that NB01, BB01, and BB02 have transmission below 250 nm. The atmosphere heavily attenuates UV light below this wavelength while traversing through the monochromator and collimator, making the signal insufficient for measurement. Also, the Xenon light source radiance increases almost linearly by 60 times between 200 nm and 300 nm, beyond which the emission is relatively flat till 400 nm. This leads to insufficient SNR in the output during photometric calibration and spectral validation for these filters.

Our results demonstrate that the measured data counts per second are within 20% of those derived from the throughput model (refer Table 4.1), except for NB07. A reason for this can be traced to using SOLSPEC data to model the throughput for wavelengths beyond 320 nm and SOLSTICE data for modeling throughputs below 320 nm. SOLSPEC has a resolution of 0.5 nm, unlike SOLSTICE data offering a resolution of 0.1 nm. This leads to lesser accuracy of the modeled data counts for filters operating beyond 320 nm. The modeled counts are not drastically different for NB08, despite lying beyond 320 nm. This can be attributed to the extremely narrow (0.1 nm) bandpass of NB08 centered at the prominent Ca II H spectral line. BB03, on the other hand, has an effective bandpass of 40 nm, which makes the model oblivious to small-scale fluctuations in the sparsely sampled SOLSPEC solar spectrum and yields similar data numbers per second to that measured in the lab.

To test this hypothesis, the lower-resolution SOLSPEC data is used to

model the throughput for the NB06 filter. This is compared to that calculated for NB06 using higher-resolution SOLSTICE data. Fig. 4.3 shows the fluctuating nature of the sparsely populated SOLSPEC spectrum in continuum regions, along with the effective bandpasses of *SUIT* in NB06 and NB07 filters. The red dotted line represents the SOLSPEC solar spectrum, while the black solid lines represent the filter throughput. Due to sparse sampling of the solar spectrum, the throughput estimation is off from the measured values. From Table 4.1, we see that the ratio of measured vs. modeled throughput for NB06 using higher resolution SOLSTICE data is 1.07. However, when the NB06 throughput is modeled using lower-resolution SOLSPEC data, the ratio obtained is $({}^{DN_{measured}}/_{\mathrm{DN_{throughput}}}) \approx 1.96$. This result is similar to what we see for NB07 throughput modeled with SOLSPEC data. Therefore, the high ratio for NB07 in Table 4.1 can be attributed to the sparsely populated SOLSPEC data used to model the throughput.

4.4 Full Payload Spectral Validation

Spectral validation aims to verify the *SUIT* payload's transmission profile with various science filters at different wavelengths within the respective filter bandpasses. Light from the monochromator is collimated and fed into the payload as before. The wavelength band of the source is chosen so that multiple measurements can be made at non-overlapping wavelength bins within the transmission band of a given filter. A holographic grating of 2400 lpmm blazed at 220 nm is used in the monochromator. The nominal dispersion of this grating is 0.74 nm/mm. The entrance slit width of the monochromator is set at 200 microns, providing a wavelength bin of 0.148 nm. This light is fed into the payload, and readings are taken across the transmission spectrum of the science filter, keeping adjacent readings independent of each other. The total energy is counted at each measured wavelength, and the spectral response of the entire telescope for the concerned filters is measured.

Following this, the entrance slit width of the monochromator is increased to 3 mm, and the light output is measured from the clear aperture of the collimator with the NIST traceable photodiode to verify the spectral flux being fed into the *SUIT* payload. This information is used to get a photometric

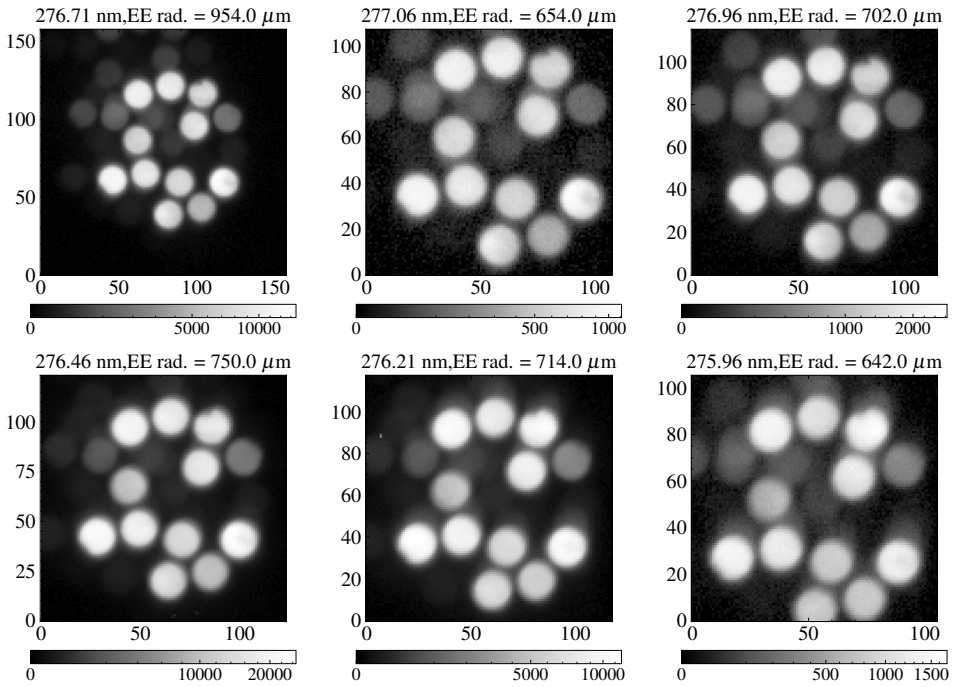

Figure 4.4: Images captured at various wavelengths for the NB02 filter of *SUIT*. The measurement wavelength and the 99% encircled energy radius are quoted at the top of each panel. The axes of the images are in pixels and the colorbar represents Data Numbers (DN).

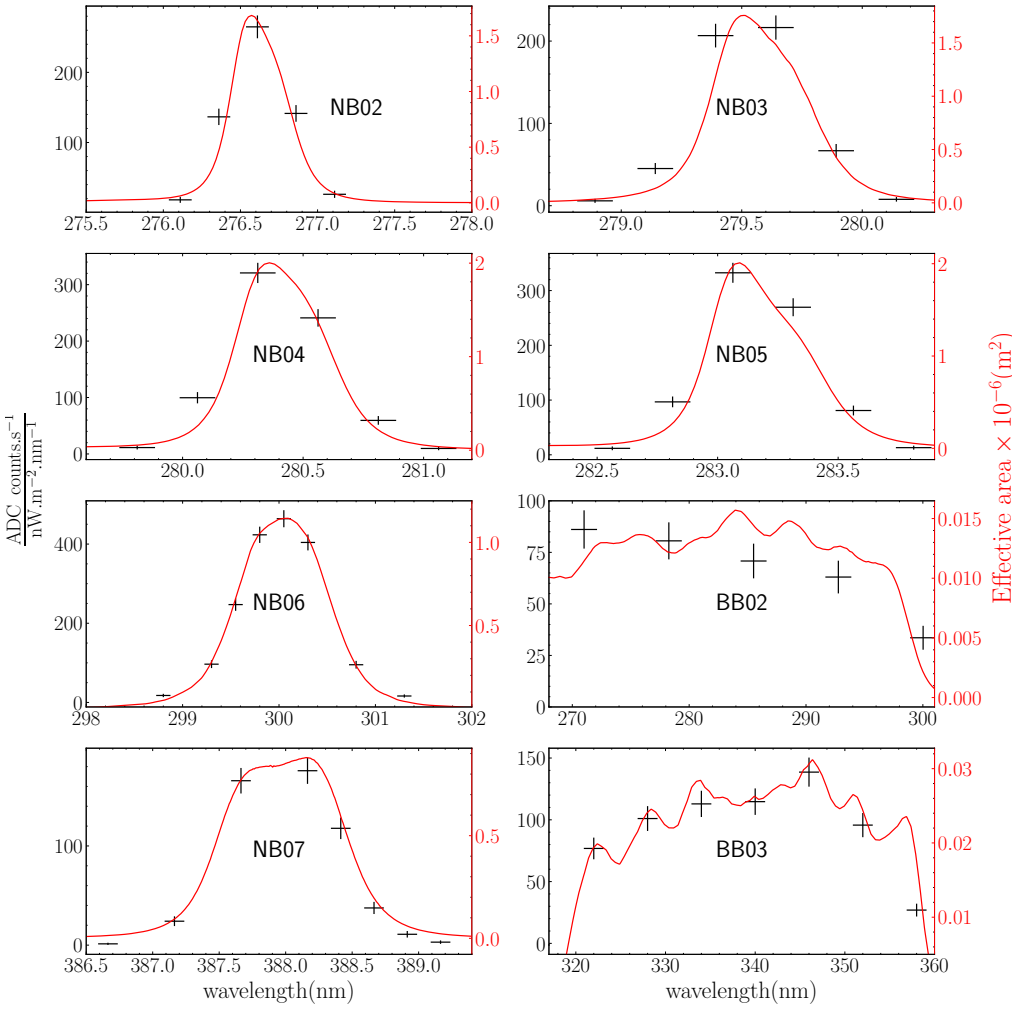

Figure 4.5: Spectral validation for various filter combinations inferred from the imaging measurements (black markers). The x-axis denotes the wavelength in nm and the y-axis denotes the ratio of ADC counts collected on the CCD with the spectral irradiance measured by the photodiode. The wavelength bins give the x errors from the given input slit size. The Poisson uncertainty of the measured ADC counts gives the y errors. The red solid curve shows the effective area calculated from measured transmission profiles of each component using Eqn 4.2.

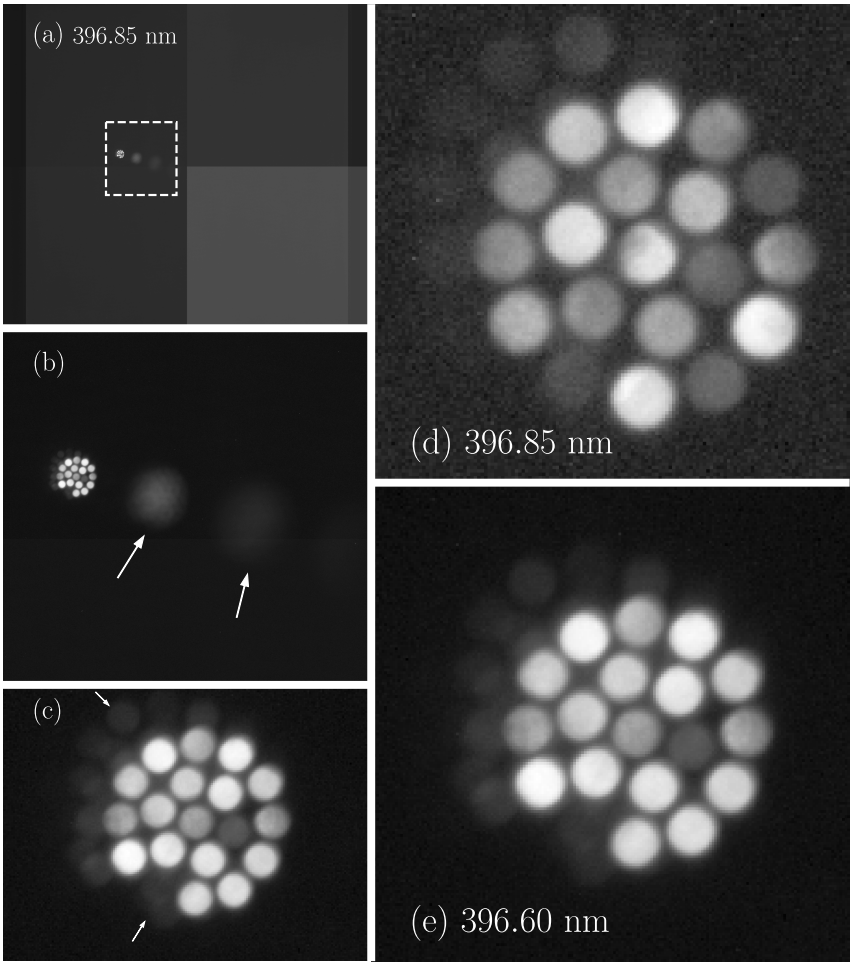

Figure 4.6: (a) The ghost reflections of the optical fiber as seen with the NB08 filter. The input beam is centered at 396.85 nm. The position of the ghost reflections is marked with a white dashed box. (b) The zoomed-in view of the white dashed box. The arrows indicate sparsely spaced ghost reflections. (c) The arrows indicate two closely spaced ghost reflections close to the center. (d) 99% encircled energy box around the fiber bundle at 396.85 nm. (e) 99% encircled energy box around the fiber bundle at 396.60 nm.

calibration to the measured spectral flux. The spectral validation is performed with the setup illustrated in Fig. 4.2. Similar to the method described in §4.4, we can estimate the spectral response of the concerned filters using the,

$$\mathrm{R}(\lambda = \lambda_1) = \frac{\mathrm{C}(\lambda = \lambda_1)}{\mathrm{E}_{\mathrm{Photodiode}}(\lambda = \lambda_1)} \text{ where,} \tag{4.4}$$

$\mathrm{R}(\lambda = \lambda_1)$ = The spectral response of a given filter at $\lambda = \lambda_1$(in units of ${}^{DN.s^{-1}}/_{\mathrm{nW.m^{-2}.nm^{-1}}}$)

$\mathrm{C}(\lambda = \lambda_1)$ = Data number per second within 99% enclosed counts radius of the fiber image at $\lambda = \lambda_1$(in units of $\mathrm{DN.s^{-1}}$)

$\mathrm{E}_{\mathrm{Photodiode}}(\lambda = \lambda_1)$ = Measured input spectral irradiance from the photodiode at $\lambda = \lambda_1$(in units of $\mathrm{nW.m^{-2}.nm^{-1}}$)

- Similar to image acquisition during photometric calibration - the fiber face is opened and closed consecutively to record light from the data and the contribution from the background at various wavelengths within the concerned filter passband.
- The median value of the background is subtracted and the total counts within the 99% enclosed energy radius ($C(\lambda_1)$) is calculated in units of $\mathrm{DN.s^{-1}}$.
- The corresponding spectral irradiance is derived by dividing the photodiode measurement ($E_{Photodiode}(\lambda_1)$) ($\mathrm{nW.m^{-2}.nm^{-1}}$) with the spectral bin size.
- This gives us the response of the concerned filter at $\lambda = \lambda_1$ with, $\mathrm{R}(\lambda_1) = \frac{\mathrm{C}(\lambda_1)}{\mathrm{E}_{\mathrm{Photodiode}}(\lambda_1)}$ (in units of ${}^{DN.s^{-1}}/_{\mathrm{nW.m^{-2}.nm^{-1}}}$)

In Fig. 4.4, we show the captured images for the NB02 filter combination at various wavelengths of incident light. The same was performed for all other

filter combinations, but is not shown here for brevity. The measurement wavelength and the calculated 99% encircled energy radius are quoted at the top of each panel. We plot the spectral validation results of all filter combinations with transmission bandpasses above 250 nm in Fig. 4.5. The x and y error bars in Fig. 4.5 represent wavelength bins for the given input slit size and the Poisson uncertainty of the measured ADC counts, respectively. The Poission uncertainty is given by the square root of the total detected photoelectrons in the image of an optical fiber. This is scaled to appropriate units while plotting.

The plots demonstrate that the measured shape of the instrument spectral response agrees well with the modeled spectral response for all filter combinations with transmission bandpass above 250 nm.

Each *SUIT* filter is mounted with a carefully chosen tilt, eliminating the possibility of inter-filter reflections as in Table 2.6. This is with the exception of NB08, where both filters are mounted without any relative angle between them, unlike other filter combinations (relative tilt of several degrees between filters). This filter has a 0.1 nm bandpass, and even slight tilts can cause a significant relative wavelength shift, potentially moving the Ca II H line out of the filter's in-band spectrum [38]. Therefore, we could not carry out the spectral characterization for the NB08 filter due to the appearance of multiple strong ghost reflections close to the central patch. In Fig. 4.6 (a), we plot the fiber image captured at 396.85 nm. The position of the central image of the fiber, along with the sparsely spaced ghost reflections, is marked with a white dashed box. Fig. 4.6 (b) shows the zoomed-in view of the box. The sparsely shaped ghost reflections are marked with white arrows. Some ghost reflections are also seen very close to the central patch. Fig. 4.6 (c) shows a zoomed-in view around the central patch, with arrows indicating two closely spaced ghost reflections. These ghost reflections appear very close to the central patch, and the relative brightness of the central patch to the ghost reflections changes as a function of wavelength, affecting the 99% encircled energy radius estimation as seen in Fig. 4.6 (d) and (e). A practical implication of this could be reduced contrast of solar features due to these ghost reflections.

4.5 Discussion & Conclusion

In this document, we present the photometric calibration and full payload spectral validation for the *SUIT* payload of Aditya-L1. The experimental setup comprises the payload maintained in an ultra-clean high vacuum environment and a collimator feeding light from a monochromator into the payload. The collimator must have high UV reflectance with comparable optical quality to the payload. Therefore, the flight spare model of *SUIT* is used for this purpose.

The intensity of collimated light within a specific wavelength band is measured with a NIST-traceable photodiode and fed into the payload. These values are compared with forward-modeled throughput derived using sun-as-a-star spectrum from SOLSTICE and SOLSPEC. Measurements are made for filters with bandpasses above 250 nm. The ratio of measured photoelectrons to that derived from the model is within 10% for NB04, NB05 and NB06 filters, within 20% for NB02 and NB08 filters, and within 30% for NB03 and BB03 filters.

The discrepancy observed in NB07 at 388 nm (see Table 4.1) is due to the sparse resolution of SOLSPEC data, which is used to model throughputs above 310 nm. A comparative analysis of the improved modeling accuracy of SOLSTICE data as compared to SOLSPEC is also demonstrated.

The above calibration is not performed for NB01, BB01, and BB02 filters as the bandpasses are below 250 nm. These wavelengths get attenuated due to O_3 formation in the atmosphere. Moreover, the Xenon light source transmission increases linearly by ≈ 60 times between 200 nm and 300 nm, beyond which the transmission is relatively flat till 400 nm. Thus, the data gathered for wavelengths below 250 nm has low SNR and is unreliable for photometry.

Each filter in the *SUIT* science filter combinations studied here has transmission outside the bandpasses mentioned in Table 1.2 in the 0.01% to 0.001% range. This prevents any out-of-band light originating anywhere outside the payload from reaching the CCD [38]. Therefore, the disagreement between the experimental results and the model is not due to spectral leakage.

For the spectral validation, the wavelength bin of the input light is reduced compared to that during photometric characterization, and the response is measured at various wavelengths across the transmission bandpass of the fil-

ters. It is seen that the spectral response of the instrument matches the wavelength bands *SUIT* is designed to observe (see Fig.4.5). We could not perform the spectral validation for the NB08 filter due to multiple ghost reflections close to the central patch.

The payload performance measured in the lab agrees well with the modeled results, validating *SUIT*'s optical performance and presenting the reliability of the developed throughput model.